Fusion Engineering and Design 87 (2012) 556–560

Contents lists available at SciVerse ScienceDirect

Fusion Engineering and Design

journal homepage: www.elsevier.com/locate/fusengdes

CFD analysis of flow boiling in the ITER first wall

Phani Domalapally[a,*], Enrico Rizzo[b], Laura Savoldi Richard[a], Fabio Subba[a], Roberto Zanino[a]

[a] Dipartimento di Energetica, Politecnico, I-10129 Torino, Italy
[b] Institut fuer Technische Physik, Karlsruhe Institute of Technology, Karlsruhe, Germany

ARTICLE INFO

Article history:
Available online 23 February 2012

Keywords:
Boiling
First wall
Two phase flow
Computational Fluid Dynamics

ABSTRACT

This paper compares two Computational Fluid Dynamic (CFD) approaches for the analysis of flow boiling inside the first wall (FW) of the International Thermonuclear Experimental Reactor (ITER): (1) the Rohsenow model for nucleate boiling, seamlessly switching to the Volume of Fluid (VOF) approach for film boiling, as available in the commercial CFD code STAR-CCM+, (2) the Bergles–Rohsenow (BR) model, for which we developed a User Defined Function (UDF), implemented in the commercial code FLUENT. The physics of both models is described, and the results with different inlet conditions and heating levels are compared with experimental results obtained at the Efremov Institute, Russia. The performance of both models is compared in terms of accuracy and computational cost.

1. Introduction

In ITER, the FW heat load during operations can be as high as several MW/m^2, which should be removed by a proper cooling system to prevent damage of the component [1]. The proposed sink to handle this load consists of copper alloy (CuCrZr) hypervapotron or swirl tubes, which exploit the large heat transfer coefficient (HTC) characteristic of highly sub-cooled boiling [2].

In order to predict the system performance, a dedicated thermal hydraulic analysis has to be conducted, and several papers have been devoted during the last few years to this task on different geometries foreseen for the ITER first wall [3–7].

Here we test and compare two approaches, based respectively on an enhancement of the Rohsenow model [8] and on the classical Bergles–Rohsenow (BR) work [9]. The first model is available in the commercial STAR-CCM+ code, including a smooth transition to the VOF model for film boiling. We implemented the second in the FLUENT code, specifically for this work. We then compared our computed results with experimental data from Efremov Institute, Russia [10].

Although our ultimate goal is to develop predictive capabilities for the hypervapotron, we start by analyzing in some detail the simpler case of a rectangular (so-called flat) channel, heated on one side. This allows us concentrating on the details of the heat transfer model performances. Preliminary results for the hypervapotron are discussed at the end of the paper.

The layout of this work is as follows: in the next section we discuss the system geometry and meshing issues. In Section 3 we describe the physical models. In Section 4 we present and discuss our results, in terms of both accuracy and numerical performance. To the best of our knowledge, this is the first time that the Rohsenow and BR models are critically compared for an ITER-relevant application. Also, we are not aware of an implementation of the BR model in FLUENT so far and, indeed, previous applications of FLUENT to ITER-relevant boiling problems met only limited success [6].

2. Geometry and mesh

Fig. 1 represents the experimental test section. It also shows the location of a set of thermocouples inserted 1.5 mm below the heated surface. Fig. 2 shows a cross-section highlighting the inner dimensions of a flat channel. In the hypervapotron case, a number of teeth are machined at the top of the fluid flow channel, along with a side channel. The hypervapotron channel dimensions are given in Fig. 3, showing cross and longitudinal sections. In both cases, the top wall is heated over a length of 100 mm, the system being otherwise thermally insulated.

For the flat-channel geometry, we tested a number of hexahedral non-uniform meshes created with the commercial mesh generator GAMBIT, ranging from 0.3 to 1.7 Mcells. We found a relative variation of the computed temperature of ∼12% (using the inlet subcooling as the reference value) when the mesh size varied from 0.3 to 1.0 Mcells. This variation was reduced to ∼2% when the mesh size went from 1 to 1.7 Mcells. Then, ∼1 Mcells are a good compromise between reasonable grid-independence of the solution and computational cost. This size of the mesh is also comparable to that chosen in previously published works on the same subject [6,7]. For the hypervapotron, we kept the same average cell size (∼0.5 mm), but we used tetrahedral cells because of the more complex flow

* Corresponding author.
E-mail address: phani.domalapally@polito.it (P. Domalapally).

0920-3796/$ – see front matter © 2012 Elsevier B.V. All rights reserved.
doi:10.1016/j.fusengdes.2012.01.024

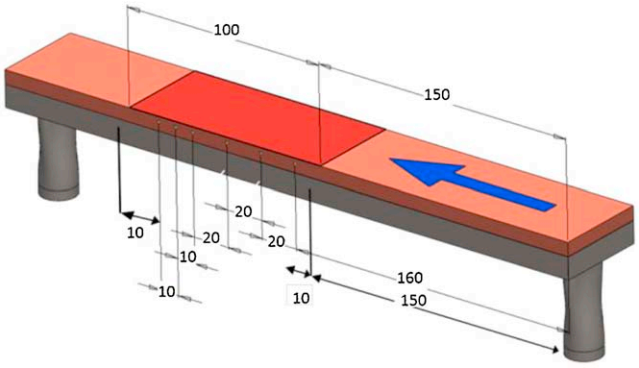

Fig. 1. 3D sketch of the experimental test section geometry (the dark region on the top marks the heated surface, all dimensions are in mm).

geometry. In both cases, left-right symmetry was assumed, i.e., the computational domain included only half of the channel.

3. Modeling

Typical experimental inlet conditions for the flat-channel are pressure p_{in} = 20 bar, temperature T_{in} = 128 °C (i.e., a subcooling of ~85 °C), V_{in} = 1–4 m/s. For the hypervapotron, they were similar except for a lower inlet temperature T_{in} = 110 °C (i.e., a stronger subcooling of ~103 °C). In these conditions, the flow was always turbulent (Reynolds number $Re \sim 5 \times 10^4$ for the lowest mass-flow rate).

Both models compared in this paper are based on the Navier–Stokes equations. Turbulent flow was accounted for by the realizable k-epsilon model, with wall-functions to handle y^+ ~30 near the wall, where y^+ is defined in [11]. In the experimental apparatus the entrance and exit ducts are orthogonal to the fluid flow in the main channel. This provides a sharp change in direction of the flow field which helps increasing turbulence. Moreover, the heated region starts ~17 hydraulic diameters after the inlet section. Consequently, we imposed fully developed flow conditions. STAR-CCM+ solves the two-phase flow field with the Eulerian approach combined with the Rohsenow model for nucleate boiling smoothly transitioning to VOF for film boiling. It includes gravity and surface tension. In contrast, FLUENT consider a single fluid (liquid), with an ad hoc prescription for the HTC in the subcooled boiling region, following the BR treatment [9]. Surface tension is not present in the model and, due to the limited density variation with temperature in the liquid phase, gravity is also not included.

Both codes were run with a pressure-based segregated solver [12]. We run STAR-CCM+ mostly in steady-state mode. A few tests (including power level higher than the experimental CHF) showed

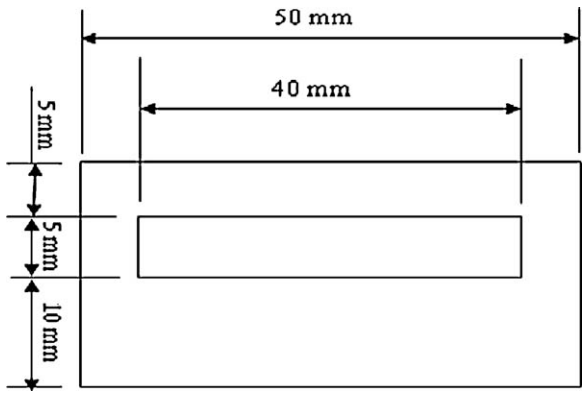

Fig. 2. Flat-channel cross-section.

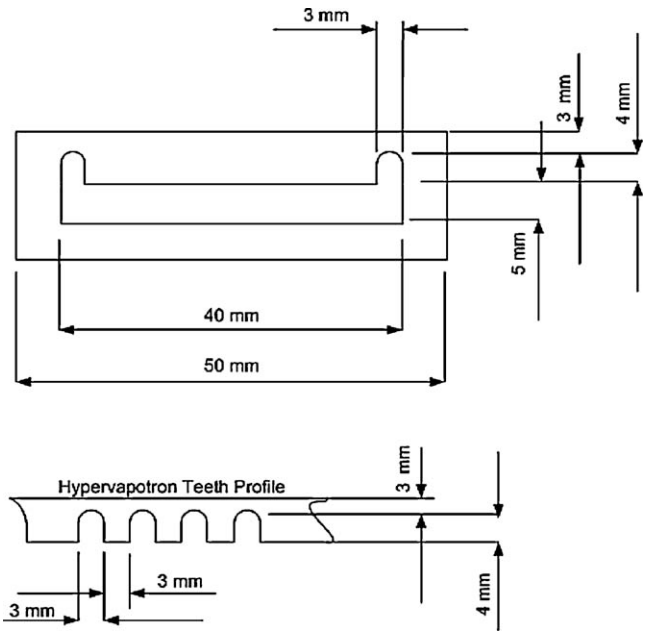

Fig. 3. Cross (top) and longitudinal (bottom) sections of the hypervapotron channel.

that transient runs led to the same solution, with a higher computational cost. In contrast, we needed to run FLUENT in transient mode, since in steady state mode it accepts prescription on the HTC at the first iteration only.

The BR model is computationally less expensive than the Rohsenow one. In fact, solving for one phase only, it saves both the memory allocation needed to store the vapor-related information and the iterations required to solve the vapor equations. Furthermore, the single-phase approach avoids sharp variations in the fluid properties, with beneficial effects on the convergence.

3.1. STAR-CCM+/Rohsenow model

The Rohsenow model implemented in STAR-CCM+ employs an empirical correlation to calculate the surface heat flux due to boiling [8]. This is given by

$$q_{bw} = \mu_l h_{lat} \sqrt{\frac{g(\rho_l - \rho_v)}{\sigma}} \left(\frac{C_{pl}(T_w - T_{sat})}{C_{qw} h_{lat} Pr_l^{n_p}} \right)^{3.03} \quad (1)$$

where μ_l is the liquid viscosity, C_{pl} is the liquid specific heat, h_{lat} is the latent heat, Pr_l is the liquid Prandtl number, $\rho_{l(v)}$ is the liquid (vapor) density, $T_{w(sat)}$ is the wall (saturation) temperature, σ is the surface tension, g is the gravity acceleration, n_p is the Prandtl number exponent and C_{qw} is a constant dependent on the liquid/surface combination. The vapor mass generation rate is given by

$$\dot{m}_{ew} = \frac{C_{ew} q_{bw}}{h_{lat}} \quad (2)$$

where C_{ew} is the heat flux fraction used to create vapor bubbles. The rate of evaporation and condensation is calculated using the formula

$$\dot{m}_{ec} = \frac{C_{HTC \times Area} \cdot (T - T_{sat})}{h_{lat}} \quad (3)$$

where $C_{HTC \times Area}$ (W/m^3 K) is the HTC between a bubble and the surrounding liquid times the contact area per unit volume, and T is the temperature of the mixture.

A VOF approach is used to track the liquid vapor interface in the film boiling regime. Switching between nucleate and film boiling is tuned by a critical value of the vapor fraction, called α_{fb}.

Table 1
Values adopted for the free parameters in the STAR-CCM+ boiling model.

C_{qw}	C_{ew}	$C_{HTC\times Area}$	α_{fb}	n_p	S_{ct}
0.01	0.01	5×10^6	0.3	1	0.5

An additional tunable parameter is the turbulent Schmidt number S_{ct}, the ratio of eddy viscosity to eddy mass diffusivity [14]. Overall, there are six user provided input parameters. Here we use the values suggested in [6,7], see Table 1, determined best-fitting the experimental database.

3.2. FLUENT/BR model

Bergles and Rohsenow [9] suggest that subcooled boiling heat transfer may be described by:

$$q_{total} = (q_{FC}^2 + (q_{FDB} - q_0)^2)^{1/2} \tag{4}$$

where q_{FC} and q_{FDB} are the forced convection and fully developed boiling heat flux, and q_0 is the flux at the onset of nucleate boiling. The boiling curve predicted by (4) merges smoothly with the forced convection curve for $q_{FDB} = q_0$, and approximates accurately the fully developed curve for $q_{FDB} \gg q_{FC}, q_0$, see Fig. 4. q_{FC} is given by the single-phase wall heat transfer model built in FLUENT. A series of tests showed that its value can be estimated by the classical Dittus–Boelter equation within 15% accuracy. q_{FDB} is given by

$$q_{FDB} = \left(\frac{T_w - T_{sat}}{C_s}\right)^3 \tag{5}$$

where C_s is a free parameter. In principle, also the exponent in Eq. (5) must be input by the user. However, the value 3 is strongly recommended [9], and we kept it frozen. A discussion of q_0 can be found in [5].

FLUENT adopts a law-of-the-wall for the near wall temperature profile y^* (Eq. (6))

$$T^* = \frac{(T_w - T_p)\rho c_p k_p^{1/2}}{\dot{q}} = \begin{cases} Pr\, y^* + \frac{1}{2} Pr \frac{C_\mu^{1/4} k_p^{1/2}}{\dot{q}} U_p^2 & (y^* < y_T^*) \\ Pr_t \left[\frac{1}{\kappa}\ln(Ey^*) + P\right] & (y^* > y_T^*) \end{cases} \tag{6}$$

where the subscript "p" means that the corresponding quantity is evaluated at the center of the near-wall cell. U is the flow velocity, κ is the von Karman constant ($\kappa = 0.4187$), E is an empirical constant ($E = 9.793$) and P is defined in [13]. The dimensionless distance y^* is defined in [15]. It serves the purpose of extending the wall function applicability to non-equilibrium boundary layers. In the case of slowly varying flow properties, as the one we are interested in, we have $y^* = y^+$. The critical value y_T^* corresponds to the intersection of the linear and logarithmic layers.

Table 2
Free parameters in the FLUENT/BR model.

	Value	Sensitivity
Pr_t	0.1	0.80
C_s	8.4e−3	0.96

Pr_t is the energy Prandtl number, which we used to tune the model as follows: Pr_t was first optimized to match the flat-channel experimental data for a reference case ($V_{in} = 2$ m/s, $Q = 1$ MW/m^2), and later C_s was tuned for $V_{in} = 2$ m/s, $Q = 2$ MW/m^2. This left the remaining part of the available experimental database free to validate the choice using fully independent information.

Table 2 summarizes the values of the free parameters used in our FLUENT/BR modeling, together with the sensitivity to their variation. The latter is defined as

$$S = \frac{(\Delta e/e)}{(\Delta x/x)} \tag{7}$$

where e is the average error produced by the model with respect to the temperature measured by the thermocouples and x the quantity against which the sensitivity is checked (either Pr_t or C_s). The high sensitivity to Pr_t is characteristic of turbulent flows at large Re, while the strong effect of C_s is due to its third power influence on q_{FDB} in (5).

4. Results and discussion

4.1. Flat channel

We analyze a subset of the experimental runs [10], see Table 3. Figs. 5–7 compare the temperatures computed at the thermocouples location with the measured values. Far from CHF, the average error (over all thermocouples) of the Rohsenow model for the case $V_{in} = 1$ m/s is 4–5 °C (~5% of the bulk fluid subcooling), and 3–4 °C (~4%) at higher Q; for the BR model it is 5–8 °C (~8%) far from CHF and 11–12 °C (~14%) approaching CHF (~4 MW/m^2). For higher V_{in} the error shows a similar behavior, with the two models having comparable accuracy for low-to-moderate heat flux and the Rohsenow approach performing better near CHF.

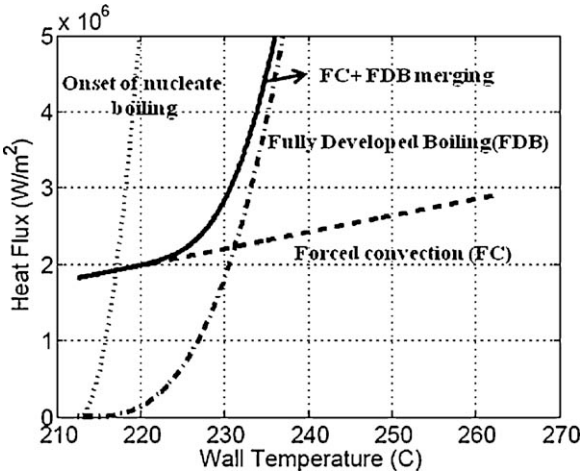

Fig. 4. Forced convection (dashed), onset of nucleate boiling (dotted), fully developed boiling (dash–dotted) heat fluxes, together with the BR merging (solid). Data are for the operating pressure of 20 bar.

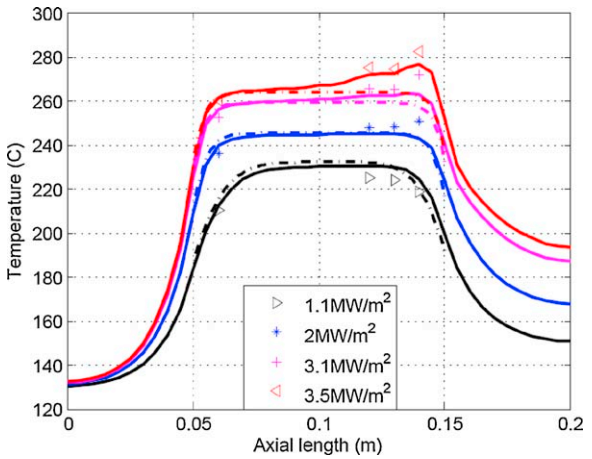

Fig. 5. Flat channel. Comparison of temperatures computed with the Rohsenow (solid line) and the BR (dash–dot line) models, with the thermocouple data (symbols) for $V_{in} = 1$ m/s and at different Q levels.

Table 3
Experimental test matrix for the flat-channel geometry.

V_{in} (m/s)	1	2	4
Q (MW/m^2)	1.1, 2, 3.1, 3.5 and 4 (CHF)	1, 2, 3, 4, 4.5 and 5 (CHF)	1, 2, 3, 4, 5, 6, 6.5 and 7 (CHF)

Underlined: simulations performed.

The error values found with the BR model are of the same order of those reported in [5], where the BR model was adopted in conjunction with the SC\TETRA code. The better behavior of the Rohsenow model approaching CHF reflects the inclusion of more detailed physics (two-phase flow), but also the larger number of free parameters which can be used to tune the model against the experimental database.

Figs. 5–7 also show that the Rohsenow model reproduces the shape of the peak in the temperature profiles at the end of the heated region for high heat fluxes (except for V_{in} = 4 m/s, suggesting that the code overestimates the drag force applied to the vapor bubbles at large flow velocities), while the BR does not. In fact, at higher heat fluxes vapor accumulates near the end of the heated region, producing a localized thermal resistance which cannot be seen by the (single phase) BR model.

Fig. 8 shows that the average vapor volume fraction (over the upper fluid–solid interface), computed using the Rohsenow model, is extremely sensitive to V_{in}, for any given Q.

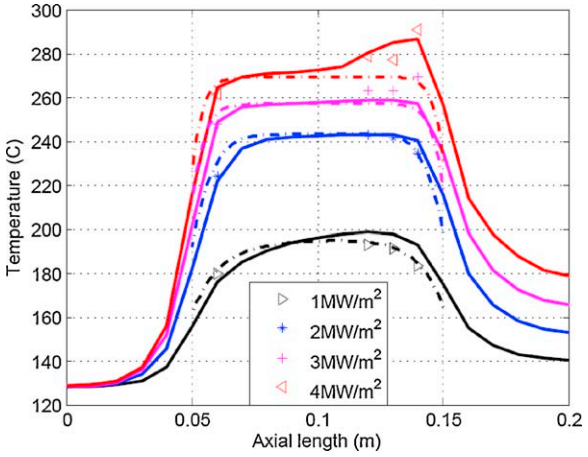

Fig. 6. Flat channel. Comparison of temperatures computed with the Rohsenow model, the BR model, and the experimental data for V_{in} = 2 m/s.

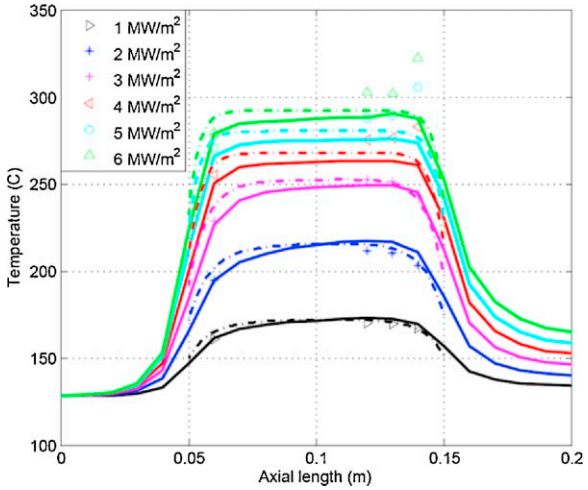

Fig. 7. Flat channel. Comparison of temperatures computed with the Rohsenow model, the BR model, and the experimental data for V_{in} = 4 m/s.

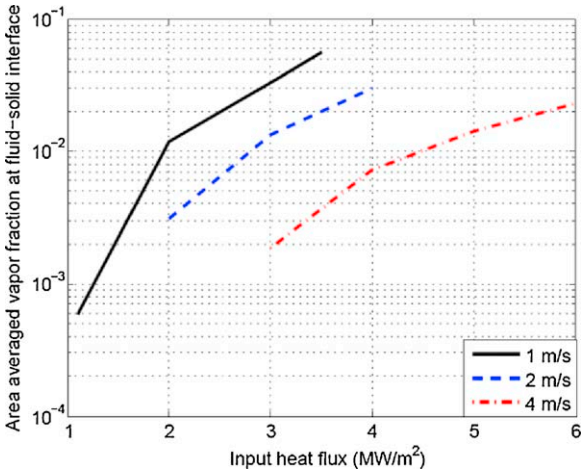

Fig. 8. Flat channel. Vapor volume fraction, averaged over the fluid–solid interface on the heated side of the flat-channel, as a function of the input heat flux. V_{in} = 1, 2, and 4 m/s are considered.

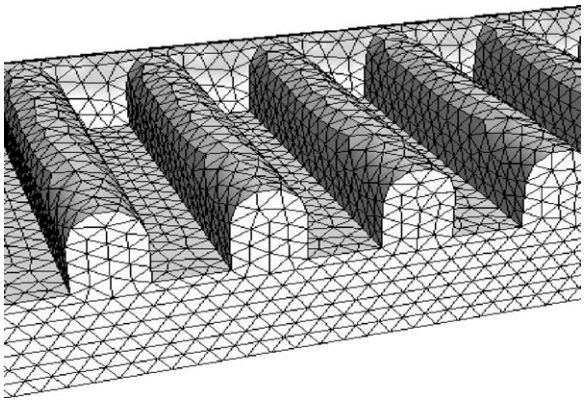

Fig. 9. Detail of the surface grid used for the hypervapotron geometry. A few teeth and the side-channel behind them are visible.

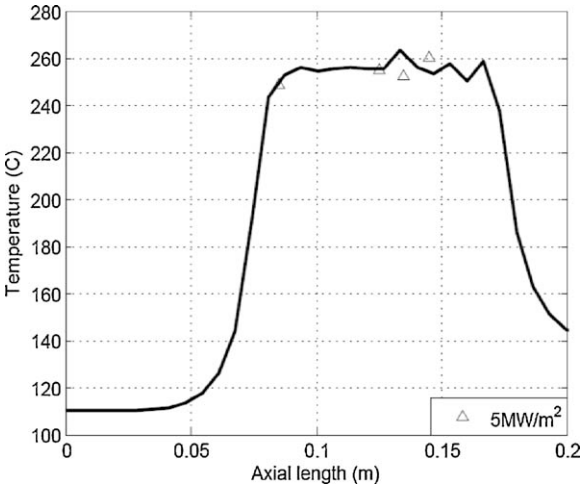

Fig. 10. Hypervapotron. Comparison of temperature profile computed by Rohsenow model with experimental data for Q = 5 MW/m^2, V_{in} = 2 m/s.

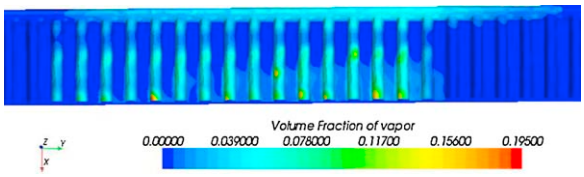

Fig. 11. Computed vapor volume fraction at the teeth top surface. $Q = 5\,MW/m^2$, $V_{in} = 2\,m/s$.

4.2. Hypervapotron

Fig. 9 shows a detail of the fluid region including a few teeth and the side channel, together with the computational (tetrahedral) mesh used for the hypervapotron. Detailed mesh-independence analysis using also other grid topologies (e.g. polyhedral) is ongoing.

Fig. 10 shows the comparison of the temperature computed by the Rohsenow model with the experimental data for the only case we tested so far, namely $V_{in} = 2\,m/s$ and $Q = 5\,MW/m^2$ (the measured CHF for this V_{in} was $\sim 9\,MW/m^2$). The average error is $\sim 5\,^{\circ}C$ ($\sim$5% of the subcooling in the bulk fluid). Fig. 11 shows the vapor volume fraction at the fingers top-surface. The accumulation of the vapor in the portion of the teeth cavities further away from the side channel is clearly visible.

5. Conclusions and perspective

We analyzed the heat transfer in highly subcooled conditions relevant for the ITER FW, in a flat-channel mock-up, comparing the Rohsenow and the BR models.

The Rohsenow model (implemented in the STAR-CCM+ code, with VOF transition for large vapor fractions) shows good agreement with the measured temperatures at all the tested input power/inlet velocity combinations, with an average error of at most $7\,^{\circ}C$ ($\sim$8% of the subcooling of the bulk fluid). The BR model behaves comparably at low-to-moderate heat fluxes, but its performance worsens approaching the CHF, due to lack of proper representation of vapor phase; the maximum average error increases to $12\,^{\circ}C$ ($\sim$14% of the subcooling).

This suggests that, notwithstanding its less detailed physics, the BR model may be a good engineering choice for first approximation analysis. In cases where more accurate information on the thermal behavior is required, or if the details of the flow field are considered a valuable output of the analysis, the Rohsenow model with transitions to VOF for film boiling should be preferred, provided a suitable experimental database is available to tune its relatively larger number of free parameters.

While the preliminary results presented here for the hypervapotron geometry suggest that the Rohsenow model can capture also in that case, as for the flat channel, the main features of the fluid flow and heat transfer phenomena, the analysis of a more extended experimental database, which is already available, will be required in the future to confirm this trend.

Acknowledgments

We thank Dr. M. Merola for reading a first draft of the paper and providing helpful suggestions, Dr. D.L. Youchison for several discussions and for kindly providing preprints of his papers, Dr. E. Baglietto for advice on the STAR-CCM+ boiling model and Dr. D. Marchisio for providing access to the computational facilities used for the present study.

References

[1] M. Merola, et al., ITER plasma-facing components, Fusion Engineering and Design 10–12 (2010) 2312–2322.
[2] A. Loarte, et al., Transient heat loads in current fusion experiments, extrapolation to ITER and consequences for its operation, Physica Scripta T128 (2007) 222–228.
[3] Y. Bournonville, et al., Numerical simulation of swirl-tube cooling concept, application to the ITER project, Fusion Engineering and Design 2–6 (2009) 501–504.
[4] S. Pascal-Ribot, et al., 3D numerical simulations of hypervapotron cooling concept, Fusion Engineering and Design 15–24 (2007) 1781–1785.
[5] A. Ying, et al., A subcooled boiling heat transfer predictive model for ITER EHF FW designs, Fusion Engineering and Design 6–8 (2011) 667–670.
[6] D.L. Youchison, et al., A comparison of two-phase computational fluid dynamics codes applied to the ITER first wall hypervapotron, IEEE Transactions on Plasma Science 387 (2010) 1704–1708.
[7] D.L. Youchison, et al., Prediction of critical heat flux in water-cooled plasma facing components using Computational Fluid Dynamics, Fusion Science and Technology 60 (2011) 177–184.
[8] W.M. Rohsenow, A method of correlation heat transfer data for surface boiling of liquid, Transactions of ASME 74 (1952) 969–976.
[9] A.E. Bergles, W.M. Rohsenow, The determination of forced convection surface boiling heat transfer, Journal of Heat Transfer 86 (1964) 365–372.
[10] I. Mazul, Russian development of enhanced heat flux technologies for ITER first wall, this conference.
[11] D.C. Wilcox, Turbulence Modeling for CFD, DCW Industries Inc., California, 1993.
[12] S.V. Patankar, Numerical Heat Transfer and Fluid Flow, Hemisphere, Washington, DC, 1980.
[13] C.L.V. Jayatilleka, The influence of Prandtl number and surface roughness on the resistance of the laminar sublayer to momentum and heat transfer, Progress in Heat and Mass Transfer 1 (1969) 193–329.
[14] STAR-CCM+ Version 6.02.008 User's Guide, CD-apdapco Inc., 2011.
[15] ANSYS-FLUENT-13.0, User's Guide, ANSYS Inc., 2010.